Materials Advances

ROYAL SOCIETY OF CHEMISTRY

PAPER

View Article Online
View Journal | View Issue

Cite this: *Mater. Adv.*, 2024, 5, 2482

Size exclusion chromatography-based length sorting of single-walled carbon nanotubes stably coated with cross-linked polymers†

Ryo Hamano,[a] Naoki Tanaka[ab] and Tsuyohiko Fujigaya *[abc]

Received 30th November 2023,
Accepted 25th January 2024

DOI: 10.1039/d3ma01069d

rsc.li/materials-advances

The stable dispersion of individual single-walled carbon nanotubes (SWCNTs) in solutions is a primary requisite for various applications, especially when their unique near-infrared (NIR) fluorescence is utilized. Coating SWCNTs with cross-linked polymers (*e.g.*, gels) can result in highly stable dispersions due to the thin gel layer that acts as an undetachable dispersant. One attractive feature of gel-coating is the design flexibility of the gel; for example, post-modifications and bioapplications are possible when reactive sites and PEG units are introduced, respectively. In this study, gel-coated SWCNTs are length-sorted using size exclusion chromatography (SEC), wherein the gel layer consists of PEG-containing gel with reactive sites. Due to the high dispersion stability of the gel coating, SEC-based length sorting is achievable without adding any dispersants in the mobile phase. The length-sorted SWCNTs obtained in this manner maintain their strong NIR fluorescence and undergo post-modification with proteins, both of which are practical for biological applications.

Introduction

Single-walled carbon nanotubes (SWCNTs) are one-dimensional nanomaterials with a high aspect ratio, ranging from tens of nm to several μm in length and several nanometers in diameter.[1–4] Their length affects their properties and assemblies, such as their optical,[5–9] mechanical,[10–12] electrical,[13–15] and dispersion properties. Therefore, understanding and controlling the length of SWCNTs is crucial to tailoring their properties for meeting the requirements of diverse applications, such as electronics, energy, and biomedical and environmental applications.

Regarding biological applications *in vivo*, the size of the nanoparticles strongly affects blood circulation, biodistribution, and selective accumulation;[16] thus, in this regard, the length of SWCNT may also be a key consideration. Indeed, SWCNT length dependency for the cell uptake efficiency was reported *in vitro*.[17,18] In addition, the unique near-infrared (NIR) adsorption and emission properties of SWCNTs that are highly permeable in the body are dependent on their length; thus, SWCNT length is one of the key factors for bioimaging[19–22] and biosensor[23–31] applications.

However, using the current SWCNT synthesis techniques, controlling the desired lengths remains challenging in the case of shorter SWCNTs. Therefore, several length sorting methods, such as density gradient centrifugation (DGU),[32,33] gel electrophoresis,[7] precipitation,[34,35] and size exclusion chromatography (SEC)[14,36–38] have been developed and utilized for various applications.[2,39,40] Among them, SEC is the most facile method for applications because the sorted SWCNT can be obtained easily by fractionation, which can be readily used for further applications, while isolation of sorted SWCNT in DGU and gel electrophoresis is challenging owing to the use of iodixanol and the gel as the media, respectively.

Length fractionation of SWCNTs by SEC is realized by the size fractionation, where the smaller particles diffuse longer distance in the pore of the stationary phase. Therefore, individual dispersion of SWCNTs and their dispersion stability are critical prerequisites for a successful SEC-based separation that can withstand the chromatography process. Therefore, SWCNTs dispersed by dispersant-based solubilization (*i.e.*, surfactant-based dispersion) is applicable only when the dispersant solutions are used as a mobile phase to maintain the equilibrium of dynamic adsorption and desorption of the dispersants in the column.[37] In this context, sodium dodecyl sulfate (SDS),[41,42] sodium cholate (SC), and sodium dodecyl cholate (SDC)[37] solutions were used as an eluent. However, owing to the toxicity of the surfactants, their removal from the sorted solutions is imperative.

[a] *Department of Applied Chemistry, Graduate School of Engineering, Kyushu University, 744 Motooka, Fukuoka 819-0395, Japan. E-mail: fujigaya.tsuyohiko.948@m.kyushu-u.ac.jp*
[b] *International Institute for Carbon Neutral Energy Research (WPI I²CNER), Kyushu University, 744 Motooka, Fukuoka 819-0395, Japan*
[c] *Center for Molecular Systems (CMS), Kyushu University, 744 Motooka, Fukuoka 819-0395, Japan*

† Electronic supplementary information (ESI) available. See DOI: https://doi.org/10.1039/d3ma01069d

On the other hand, DNA-dispersed SWCNTs (DNA/SWCNTs) are a unique system that allows the application of SEC-based length sorting owing to their dispersion stability without using any surfactants.[15,36,38,43–45] To date, length-dependent photoluminescence lifetime[43] and cellular uptake[46] have been investigated using length-sorted DNA/SWCNTs. However, critical issues with the DNA/SWCNTs include the risks of aggregation in the blood[25,47] and the replacement of the DNA with intercellular proteins.[48] Therefore, length sorting of the SWCNT hybrid with improved coating stability and biocompatibility is desired.

In this study, we investigated the sorting of the SWCNT coated by cross-linked polymer (*e.g.*, gel) prepared by CNT micelle polymerization without using surfactant in the mobile phase. In CNT micelle polymerization,[49–56] a thin gel layer (~1 nm)[51] is formed on the surface of SWCNTs by radical polymerization; moreover, the coated gel layer is free from detachment from the SWCNTs despite the excess amount of the competitive adsorbents.[51] Therefore, higher dispersion stability such that the chromatography process can be expected. Another advantage of CNT micelle polymerization is the monomer versatility; thus, biocompatibility can be achieved using biocompatible monomers such as polyethylene glycol methacrylate (PEGMA).[51,56] In addition, post-functionalization is also possible by employing maleimide-containing monomers into the gel layer,[52] and also a brighter photoluminescence (PL) of SWCNT (E_{11}^{*}) compared to the original PL (E_{11}) can be created at a longer wavelength >1100 nm by the radical grafting on SWCNTs.[53,57] Armed with these features, gel-coated SWCNTs have been used for cancer cell recognition and NIR photothermal therapy *in vitro*,[56] gene transfer into plant tissues *in vivo*,[54] and NIR live imaging of blood circulation *in vivo*.[57] Therefore, length sorting of the gel-coated SWCNTs enables the full use of these unique features for length-dependent biological studies, including tumor targeting that is highly size-dependent.

Experimental

Materials

SWCNTs (CoMoCAT, Lot#MKBZ1159V, Sigma-Aldrich Co. LLC, Saint Louis, USA), sodium dodecyl sulfate (SDS), polyethylene glycol methacrylate (PEGMA; M_n ~ 500), maleimide, furan, bovine serum albumin (BSA), and ×100 TE buffer solution (pH 8.0) were purchased from Sigma-Aldrich (Tokyo, Japan). Deuterated water (D_2O) was purchased from Cambridge Isotope Laboratories, Inc. (Tewksbury, MA). *N*,*N*′-methylenebisacrylamide (BIS), tetramethylethylenediamine (TMEDA), and ammonium persulfate (APS) were purchased from Wako Pure Chemical Industries, Ltd (Tokyo, Japan).

Synthesis of *endo*-FpMMA

Methacrylate carrying the *endo*-form of furan-protected maleimide (denoted as *endo*-FpMMA, Fig. 1) was synthesized according to the reported procedure.[52] First, the maleimide was briefly protected with furan using a Diels–Alder reaction at 25 °C, and the *endo*-form furan-protected maleimide was coupled with PEGMA using the Mitsunobu reaction to afford *endo*-FpMMA.

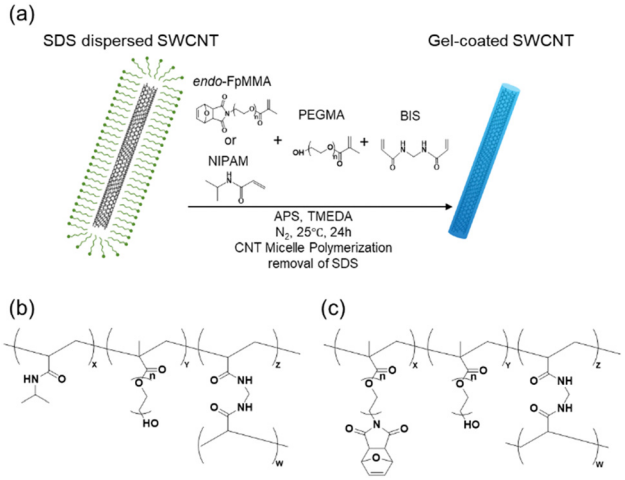

Fig. 1 (a) Scheme of the synthesis of gel-coated SWCNTs by CNT micelle polymerization. Chemical structure of the cross-linked polymer in (b) PNIPAM/PEG/SWCNTs and (c) *endo*-FpM/PEG/SWCNTs.

Preparation of SWCNT dispersion using SDS

SWCNTs (5.0 mg) and a D_2O (10 mL) solution containing SDS (2.0 wt%) were added to a 50 mL glass bottle. The mixture was sonicated using a bath-type sonicator (Branson 5510) for 1 h and a tip-type sonicator (UD-200, Tomy) for 30 min. The dispersion was centrifuged at 147 000*g* (Hitachi Himac, CS 150 GX) for 4 h, and the supernatant (top 90%) was collected. The solutions were diluted 10 times with D_2O to prepare a 0.2 wt% SDS dispersed SWCNT solution.

CNT micelle polymerization

For the synthesis of *endo*-FpM/PEG/SWCNTs, *endo*-FpMMA (60 mg, 10.5 mM), PEGMA (60 mg, 24 mM), and BIS (0.2 mg, 0.26 mM) were added to the SDS (0.2 wt%) dispersed SWCNT solution (5.0 mL), and the resulting mixture was bubbled with N_2 gas to remove O_2 for 30 min. TMEDA (8.8 μL) and a 20 wt% aqueous solution of APS (25 μL) were added to the mixture. Polymerization was conducted at 25 °C for 24 h under a N_2 atmosphere. The supernatant obtained was filtered (MWCO: 200 000) seven times to remove SDS. For the synthesis of PNIPAM/PEG/SWCNTs, NIPAM (220 mg, 38.9 mM), PEGMA (140 mg, 5.6 mM), and BIS (2 mg, 0.26 mM) were added to the 0.2 wt% SDS dispersed SWCNT solution (50 mL), and the resulting mixture was bubbled with N_2 gas for 30 min. TMEDA (88 μL) and a 20 wt% aqueous solution of APS (250 μL) were added to the mixture. Polymerization was conducted at 25 °C for 24 h under a N_2 atmosphere. The supernatant obtained was filtered (MWCO: 200 000) seven times to remove SDS.

Size-exclusion chromatography fractionation

For length fractionation of gel-coated SWCNTs, three columns with COSMOSIL CNT-300, CNT-1000, and CNT-2000 SEC columns (Nacalai Tesque, Inc.) were used in series. On the

analytical scale, columns of 10 mm (inner diameter) × 300 mm (length) were used, connected to a HPLC system (Shimadzu Corporation, Kyoto, Japan), with a flow rate of 1.0 mL min^{-1}, an injection volume of 200 μL of SWCNT dispersion, a fractionation volume of 2.0 mL per fraction, and a monitor absorption wavelength of 290 nm and 573 nm. On the preparative scale, columns of 20 mm (inner diameter) × 300 mm (length) were connected to a HPLC system (Japan Analytical Industry Co., Ltd Tokyo, Japan) with a flow rate of 2.0 mL min^{-1}, an injection volume of 5 mL of SWCNT dispersion, a fractionation volume of 4.0 mL per fraction, and a monitor absorption wavelength of 290 nm. TE buffer (containing 10 mM with pH 8 Tris–HCl and 1 mM EDTA) was used as the mobile phase. The aqueous gel-coated SWCNT dispersion was adjusted to the same pH as the mobile phase with ×100 TE buffer and filtered through a 0.45 μm filter before injection.

Measurements

The UV-vis-NIR spectra were measured at 25 °C using a V-670 spectrophotometer (JASCO, Tokyo, Japan). Photoluminescence (PL) spectra were measured using a NanoLOG-EXT spectrofluorometer (Horiba JOBIN YVON, Longjumeau, France). Absorption and PL measurements were obtained using an optical cell with an optical path length of 10 mm. Raman spectra were measured using a RAMAN touch spectrophotometer (Nanophoton, Osaka, Japan) with a 20× objective, an excitation wavelength of 532 nm, a laser power of 10 mW, an exposure time of 2 s, and five times integration at 25 °C. AFM measurements (AC mode) were performed using an Agilent 5500 probe microscope (Agilent Technologies, California, USA) in air and used for the silicon cantilever PPP-NVSTR-W (NANOSENSORS, NanoWorld AG, Neuchatel, Switzerland). For the AFM sample preparation, cleaved mica was soaked in a solution of 5 mL of 2-isopropanol and 50 μL of 3-aminopropyltriethoxysilane (APTES), allowed to stand for one hour, washed with water, and dried in air.[58] 10 μL SEC fractionated eluents were dropped onto the APTES-modified mica, allowed to stand at room temperature for 10 min, rinsed with 1 mL of water, and dried in air. AFM image processing and SWCNT length measurements were performed using the Scanning Probe Image Processor (Ver. 6.2.6).

Estimation of SWCNT concentration

The molar concentration of SWCNTs (c_{SWCNT}) was estimated using the following equation according to previous studies.[59,60]

$$c_c = 5.1 \times 10^{-8} \times \frac{\Delta_{fwhm} \times OD_{S_1}}{0.01 \times d}$$

$$c_{SWCNT} = \frac{c_c}{N_c} = \frac{c_c}{l_{SWCNT} \times N_{c/nm}}$$

where c_c [M] is the carbon concentration, Δ_{fwhm} full width at half maximum of the S_1 absorption spectrum of (6, 5)-SWCNT, OD_{S_1} is the S_1 absorbance of (6, 5)-SWCNT, d [mm] is the optical path length, N_c is the number of carbon atoms in the SWCNT, l_{SWCNT} is the average length of the SWCNT, and $N_{c/nm}$ is the number of carbon atoms per nm of SWCNT (88 for (6, 5)-SWCNT). Δ_{fwhm} and OD_{S_1} were obtained by peak separation of absorption spectra measured using package Multi Peak Fitting in Igor Pro (Ver. 6.36J).

Post functionalization of length-sorted *endo*-FpM/PEG/SWCNTs

Fr1 of *endo*-FpM/PEG/SWCNTs in PBS buffer (pH 7.4, 450 μL) was heated at 80 °C for 1.5 h to deprotect maleimide. 50 μL bovine serum albumin (BSA) solution (in PBS, 0.1 mg mL^{-1}) was added in this solution to 0.01 mg mL^{-1} and gentle shaken at room temperature for 24 h. Next, the solution was filtered through an Amicon Ultra (MWCO: 100 kDa) to remove unbound excess BSA five times. As a control experiment, *endo*-FpM/PEG/SWCNTs without heat treatment was mixed with BSA using the same procedure.

Results and discussion

SEC fractionation of gel-coated SWCNTs

Gel-coated SWCNTs were prepared by CNT micelle polymerization according to previous reports (Fig. 1(a)).[52,56]

For CNT micelle polymerization, radical polymerization using vinyl monomers was performed in SDS-dispersed SWCNT solution in the presence of *N*,*N*′-methylene bisacrylamide (BIS), and ammonium persulfate (APS) as a cross-linker and initiator, respectively. Two co-polymer systems were selected as the model coating gels: *N*-isopropylacrylamide (NIPAM) with polyethylene glycol methacrylate (PEGMA) (PNIPAM/PEG)[51] and *endo*-FpMMA with PEGMA (*endo*-FpM/PEG),[52] used in previous studies. Polymerizations were conducted at 25 °C for 24 h for PNIPAM/PEG-coated SWCNTs (PNIPAM/PEG/SWCNTs, Fig. 1(b)) and *endo*-FpM/PEG-coated SWCNTs (*endo*-FpM/PEG/SWCNTs, Fig. 1(c)). TMEDA and APS were used to lower the radical generation temperature for the *endo*-FpM/PEG system to prevent the deprotection of the fran group.[52] Surfactants were removed by repeating filtration until the ^{1}H NMR signals from the surfactant disappeared. The dispersions were stable despite the absence of the surfactant (Fig. S1, ESI†), indicating the stable coating of the gel with hydrophilic PEG units and the negative charge derived from the APS.[51]

Fig. 2 shows chromatograms of the gel-coated SWCNTs monitored at 290 nm (black line) and 573 nm (red line). For *endo*-FpM/PEG/SWCNTs (Fig. 2(a)), a unimodal peak and a bimodal peak were observed at 573-nm and 290-nm monitoring, respectively. The peak profile observed at 290 nm is similar to that of DNA/SWCNTs.[43,44,61,62] At 573 nm, there is the absorption of SWCNTs for E_{22} transition of SWCNTs with (6, 5)-chirality,[37] while at 290 nm, both SWCNTs and the protected-maleimide moiety in the *endo*-FpM monomer have absorption.[63] Therefore, the first peak (25–30 min) can be assigned to the fraction of *endo*-FpM/PEG/SWCNTs, while the 2nd peak (35–40 min) can be considered to be the fraction contained only *endo*-FpM/PEG without SWCNTs. In the CNT micelle polymerization, gel particles without SWCNTs (free gel) were formed.[49–56]

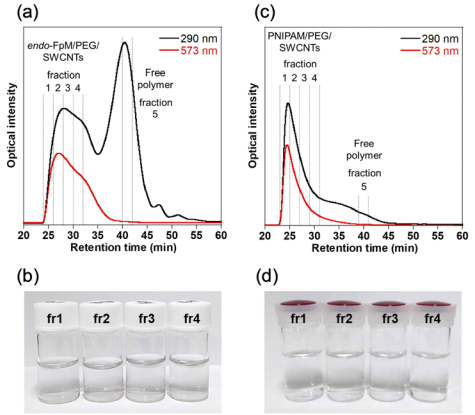

Fig. 2 (a), (c) SEC chromatograms and (b), (d) photographs of fractionated solutions of (a), (b) *endo*-FpM/PEG/SWCNTs and (c), (d) PNIPAM/PEG/SWCNTs.

Therefore, the result indicates the removal of the free gels from the dispersion is possible by fractionation in SEC-based sorting. Previously, we reported that the separation of the free gel was possible by ultracentrifugation; however, this method caused the shortening of the SWCNT owing to the strong shear force of the ultracentrifugation.[49] Contrarily, SEC-based separation is advantageous in its structural intactness for SWCNTs. For PNIPAM/PEG/SWCNTs (Fig. 2(c)), only unimodal peak was observed for both 290-nm and 573-nm monitoring. The absence of the 2nd peak after 35 min corresponds to the weak absorption of PNIPAM and PEG at this wavelength (Fig. S2, ESI†).

To analyze the size of the *endo*-FpM/PEG/SWCNTs and PNIPAM/PEG/SWCNTs after the SEC, the eluents were fractionated every 2 min, and these are denoted as fr1, fr2, fr3, fr4, and fr5. Fig. 3 shows the AFM images of the eluents, where the AFM image of the unsorted solution was also displayed as a comparison. The needle-like structure of SWCNTs was clearly observed for fr1–fr4; however, only spherical particles were observed for fr5. The result clearly supports the separation of gel-coated SWCNTs from the free gels by SEC. Importantly, the successful SEC-based separation of SWCNT without using surfactants in the mobile phase indicates a stable coating by the gel without any dynamic detachment. For *endo*-FpM/PEG/SWCNTs, SWCNT length in fr1, fr2, fr3, and fr4 were 389.7 ± 111.6 nm, 234.2 ± 72.5 nm, 154.8 ± 35.9 nm, and 103.2 ± 49.0 nm, respectively; however, that of unsorted *endo*-FpM/PEG/SWCNTs was 223.4 ± 136.0 nm (Fig. 3(a)). For PNIPAM/PEG/SWCNTs, SWCNT length in fr1, fr2, fr3, and fr4 was 354.9 ± 101.4 nm, 248.2 ± 85.8 nm, 174.8 ± 87.4 nm, and 128.9 ± 96.2 nm, respectively. However, that of unsorted PNIPAM/PEG/SWCNTs was 235.9 ± 146.0 nm (Fig. 3(b)).

The length distribution of gel-coated SWCNTs (100–500 nm) was similar to that of DNA/SWCNTs (100–500 nm).[44] We consider that the sonication treatment of the SWCNT and the filtration of the dispersion through the 0.45-μm membrane prior to the injection regulate the upper limitation of the length. The average height of unsorted gel-coated SWCNTs was 1.82 ± 0.60 nm and 1.96 ± 0.49 nm for *endo*-FpM/PEG/SWCNTs and PNIPAM/PEG/SWCNTs, respectively, while that of the free gel was *ca.* 1.0 nm. Assuming that the average diameter of CoMoCAT-SWCNTs was 0.78 nm, and the average thickness of the gel layer can be estimated *ca.* 1.0 nm,[49] indicating that the gel layer is thin and homogeneously coated on the SWCNTs.

In the absorption spectra of the unsorted and fractionated (fr1–fr5) *endo*-FpM/PEG/SWCNTs (Fig. 4(a)) and PNIPAM/PEG/SWCNTs (Fig. 4(b)), clear NIR absorption peaks were observed, and longer SWCNTs showed stronger optical absorption intensity. For fr5, the NIR absorption characteristic of SWCNTs (>1000 nm) was not observed owing to the absence of the SWCNTs. Based on the deconvoluted peak area of the (6,5)-SWCNT absorption, the concentrations of *endo*-FpM/PEG/SWCNTs of fr1–fr4 were estimated to be 0.1–0.2 nM, which is 50 times lower than injected dispersions (6.76 nM, Table S1, ESI†). Higher concentrations of NIPAM/PEG/SWCNTs fractions can be attributed to the higher injection concentration (27.9 nM). The narrower width at half maximum of the chromatogram peaks of *endo*-FpM/PEG/SWCNTs than that of NIPAM/PEG/SWCNTs (Fig. S3 and Table S2, ESI†) suggests a higher size separation resolution for a lower SWCNT concentration.

The fact corresponds to the smaller standard deviation of the length distribution of *endo*-FpM/PEG/SWCNTs (for fr3 and fr4) in AFM measurements (Fig. 3(b)). Fig. 4(c) and (d) show photoluminescence (PL) counterplots of unsorted and sorted dispersions for *endo*-FpM/PEG/SWCNTs (Fig. 4(c)) and PNIPAM/PEG/SWCNTs (Fig. 4(d)). Clear emissions of semiconducting SWCNTs were observed in all fractions, indicating that the fractionated dispersions contained individually isolated SWCNTs. The PL intensity of the sorted dispersions was maintained for more than four months, evidencing the stable coating of the gel offers excellent dispersion stability (Fig. S4–S6, ESI†). Based on the intensity of the spots, the relative distribution of chirality for the fractions was analyzed (Fig. S7 and Table S3, ESI†). We found that SWCNTs with a large diameter, such as (7, 5) and (7, 6), were enriched in shorter fractions, such as fr4; however, the content of SWCNTs with smaller diameters, such as (6, 4) and (8, 3) was decreased. Enrichment of the (7, 5) in shorter SWCNTs was also observed for absorption spectra, where the (7, 5) peak at approximately 1050 nm for (6, 5) became larger in fr3 and fr4 (Fig. S6, ESI†). Heller *et al.* reported a similar diameter dependency of the length-sorted SWCNT in both in gel electrophoresis and SEC-based sorting.[7] They considered that SWCNTs with a larger diameter contained more defects and must be cut during sonication. In AFM image analysis of *endo*-FpM/PEG/SWCNTs, the average heights of fr1, fr2, fr3, and fr4 were 1.46, 1.51, 1.57, and 1.62 nm, respectively (Fig. S8, ESI†), which supports the shorter SWCNT fraction contains a larger diameter of SWCNT.

Based on the ratio of the integral of the E_{11} emission peak area at 570 nm excitation to the integral of the E_{22} absorbance peak, the relative quantum yield[5,7] was evaluated for (6,5)-SWCNTs. Fig. 4(e) and (f) plot the relative quantum yield as a function of the average SWCNT length. The longest SWCNTs exhibited the highest relative quantum yield. The result can be

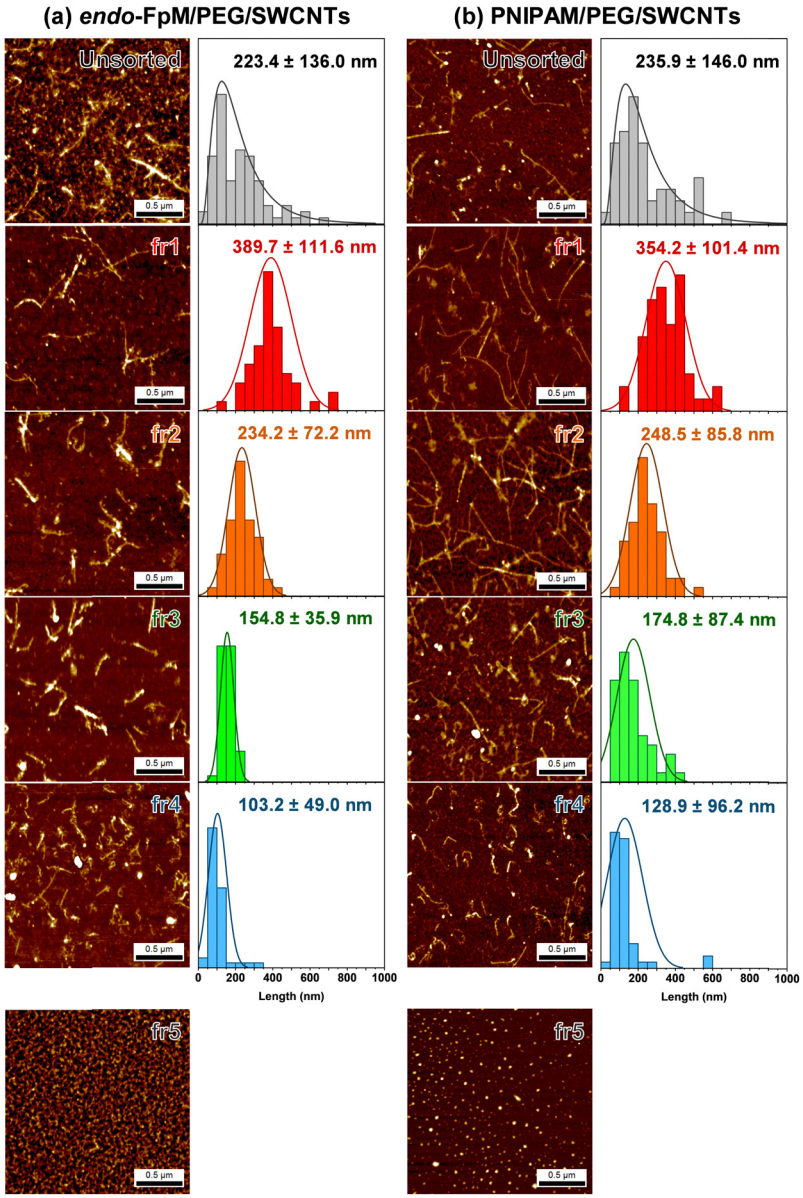

Fig. 3 AFM images and length distribution of unsorted, fr1, fr2, fr3, fr4, and fr5 of (a) *endo*-FpM/PEG/SWCNTs and (b) PNIPAM/PEG/SWCNTs. Displayed values are mean length ± standard deviation for N = 50.

explained by the lower concentration of the terminal defects at the tube ends acting as the quenching sites for the longer SWCNTs.[5,7,8] The relative quantum yield of unsorted SWCNTs lay between the lowest and highest yield, indicating that the PL intensity was the average of the SWCNTs with different relative quantum yields. Lower defect density for the longer SWCNTs was indicated by the lower D-band intensity with reference to G-band intensity at 1580 cm^{-1} (D/G ratio) in the Raman spectroscopy of *endo*-FpM/PEG/SWCNTs (Fig. 4(g), (h), and Table S4, ESI†) and PNIPAM/PEG/SWCNTs (Fig. 4(i), (j), and Table S4, ESI†).[6,64]

Noted that, in PNIPAM/PEG/SWCNTs (Fig. 4(d)), bright E_{11}^{*} luminescence owing to low-density sp^3 defects, the so called quantum defects,[65] or local functionalization was observed at 1120 nm for both the unsorted and fractionated dispersions. These sites were created by the radical grafting on the SWCNT sidewall[53,57] as indicated by the larger D/G ratios observed in PNIPAM/PEG/SWCNTs (Fig. 4(j)) than those of *endo*-FpM/PEG/SWCNTs (Fig. 4(h)). High relative quantum yields were observed for the longest SWCNT fraction and the shortest SWCNT fraction. The reason of such a high yield for the shortest SWCNTs is probably due to the overwrapping of the E_{11} luminescence from the other chirality, such as (8,4)-SWCNTs.

Post functionalization of length-sorted *endo*-FpM/PEG/SWCNTs

To demonstrate the usefulness of the sorted SWCNT dispersions for biological applications, protein conjugation was conducted using sorted *endo*-FpM/PEG-SWCNTs *via* an ene-thiol addition reaction between the maleimide group and the thiol

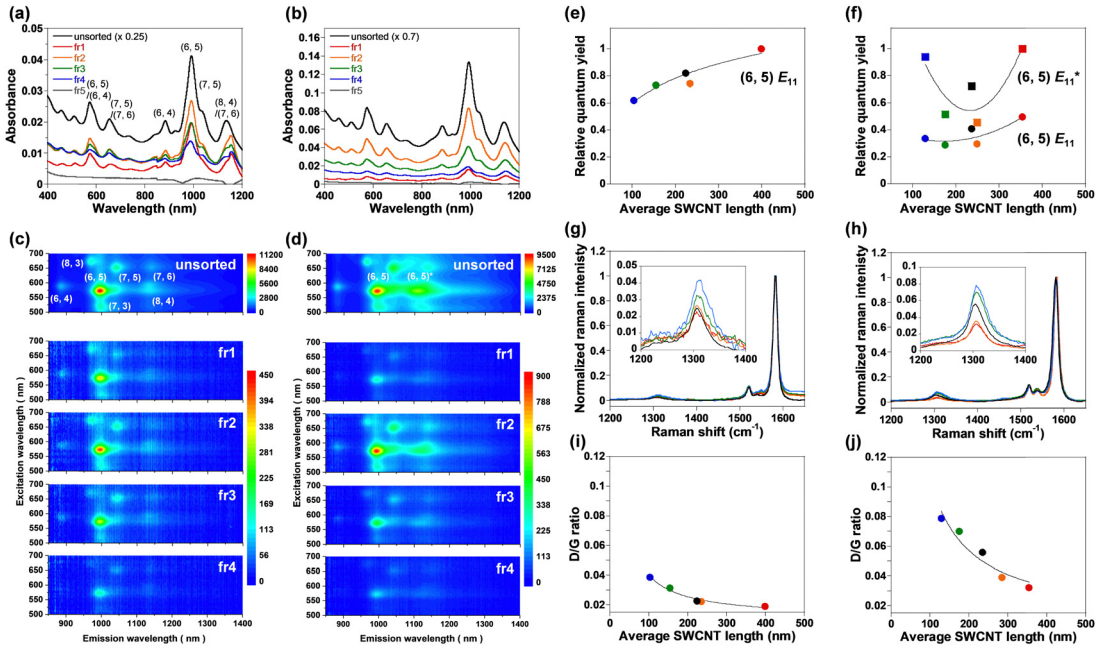

Fig. 4 Absorption spectra of unsorted (black), fr1 (red), fr2 (orange), fr3 (green), fr4 (blue), and fr5 (gray) of (a) *endo*-FpM/PEG/SWCNTs and (b) PNIPAM/PEG/SWCNTs dispersions. For comparison, absorption spectra of the unsorted dispersions are also displayed. PL counter plots of unsorted, fr1, fr2, fr3, and fr4 of (c) *endo*-FpM/PEG/SWCNTs and (d) NIPAM/PEG/SWCNTs dispersions. Chiral indices of the spots were assigned as (*n*, *m*) and PL from E_{11}^{*} was represented as (*n*, *m*)*. Relative quantum yields of (6, 5)-SWCNT of (e) *endo*-FpM/PEG/SWCNTs and (f) PNIPAM/PEG/SWCNTs as a function of average SWCNT length for fr1 (red), fr2 (orange), fr3 (green), fr4 (blue), and unsorted (black). Circles and squares represent E_{11} and E_{11}^{*} respectively, and curves are a guide to the eye. Raman spectra of unsorted (black), fr1 (red), fr2 (orange), fr3 (green) and fr4 (blue) of (g) *endo*-FpM/PEG/SWCNTs and (h) PNIPAM/PEG/SWCNTs. The inset graph is detailed near the D-band. Relationship of average SWCNT length to D/G ratio of unsorted (black), fr1 (red), fr2 (orange), fr3 (green) and fr4 (blue) of (i) *endo*-FpM/PEG/SWCNTs and (j) PNIPAM/PEG/SWCNTs. Curves are displayed as a guide to the eye.

group in the protein (Fig. 5(a)). As the model protein, bovine serum albumin (BSA) was conjugated, where fr1 was used for the conjugation. Fig. 5(b) shows an AFM image of the *endo*-FpM/PEG-SWCNTs treated with BSA. The several spots having a height of 4–8 nm, corresponding to the size of BSA,[58,66] were clearly observed along with *endo*-FpM/PEG/SWCNTs with deprotection treatment. However, no such structure was observed for *endo*-FpM/PEG/SWCNTs without deprotection treatment (Fig. S9, ESI†). We confirmed the absorption peaks derived from BSA (280 nm) and SWCNTs in the absorption spectrum (Fig. 5(c)) together with NIR PL (Fig. 5(d)) of the sample after BSA modification. These results manifest the fractionated *endo*-FpM/PEG/SWCNTs are ready for the post-functionalization and the post-modified hybrid are applicable for NIR imaging.

Scale up to the preparative scale

The volume of the injection was successfully scaled up from 200 μL to 5.0 mL by increasing the column diameter from 10 mm to 20 mm. The volume of the total fractions was increased to 40 mL per 5 injections (Fig. S10, ESI†) while maintaining the comparable SWCNT concentration in the fractions (Fig. S11 and Table S1, ESI†) and length-dependent NIR PL (Fig. S12, ESI†). In large-scale fractionation, finer fractionation was possible and the SWCNT lengths of 479.9 ± 167.4 nm, 300.0 ± 100.9 nm, 261.3 ± 100.7 nm, 226.9 ± 73.6 nm, 169.9 ± 50.2 nm, 121.8 ± 27.8 nm, and 76.5 ± 26.9 nm were obtained (Fig. S13, ESI†). This remarkable scalability of the SEC-based length sorting of gel-coated SWCNTs enables the use of *endo*-FpM/PEG/SWCNTs for practical length-dependent studies.

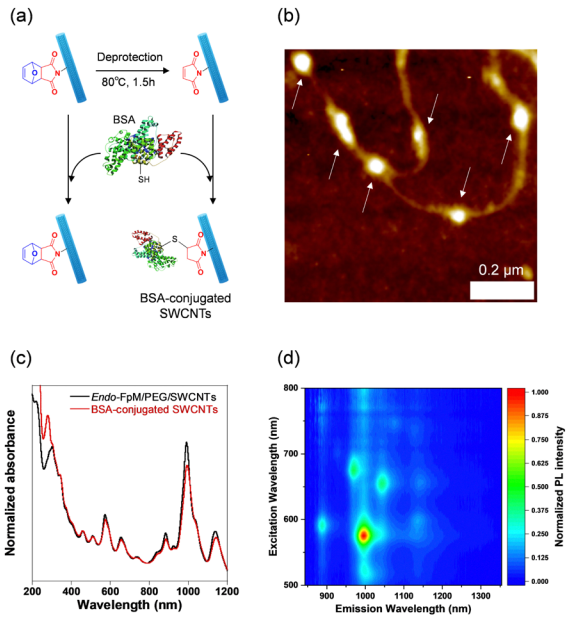

Fig. 5 (a) Schematic of BSA modification experiments on *endo*-FpM/PEG/SWCNTs. (b) Representative AFM image of BSA-conjugated SWCNTs. (c) Normalized absorption spectra of *endo*-FpM/PEG/SWCNTs before (black) and after (red) the BSA conjugation. (d) PL contour plot of *endo*-FpM/PEG/SWCNTs after BSA conjugation.

Conclusions

In this study, we successfully sorted gel-coated SWCNTs by length using size exclusion chromatography (SEC) without using a dispersant solution as the mobile phase owing to the excellent coating stability of the gel layer. SWCNT with two different chemical compositions (*endo*-FpM/PEG/SWCNTs and PNIPAM/PEG/SWCNTs) were sorted, demonstrating that the sorting can be applied independent of the gel composition. Both gel-coated SWCNTs showed bright PLs more than four months after the fractionation, indicating the high dispersion stability of the gel-coated SWCNTs. The longest gel-coated SWCNT fractions showed the highest relative quantum yields because of the lowest defect concentration. We demonstrated that post-functionalization of length-sorted *endo*-FpM/PEG/SWCNTs is possible. The gel-coated SWCNTs sorted by SEC can be readily used in biological applications, which will pave the way for length-dependent studies *in vitro* and *in vivo* to analyze and control interactions between SWCNTs and organisms.

Author contributions

Ryo Hamano: conceptualization, data curation, investigation, methodology, formal analysis, writing – original draft, funding acquisition. Naoki Tanaka: result discussion. Tsuyohiko Fujigaya: conceptualization, project administration, result discussion, supervision, writing – review & editing, funding acquisition. The manuscript was written through the contributions of all authors. All authors have given approval to the final version of the manuscript.

Conflicts of interest

There are no conflicts to declare.

Acknowledgements

This study was supported in part by Data Creation and Utilization-Type Material Research and Development Project (grant Number JPMXP1122714694) of the MEXT and the Advanced Research Infrastructure for Materials and Nanotechnology in Japan (ARIM) of the MEXT (grant Number JPMXP1222KU1007). H.R is thankful for a Grant-in-Aid for JSPS Fellows (no. 22J22541).

Notes and references

1 S. Kruss, A. J. Hilmer, J. Zhang, N. F. Reuel, B. Mu and M. S. Strano, Carbon nanotubes as optical biomedical sensors, *Adv. Drug Delivery Rev.*, 2013, **65**(15), 1933–1950.

2 F. Yang, M. Wang, D. Zhang, J. Yang, M. Zheng and Y. Li, Chirality Pure Carbon Nanotubes: Growth, Sorting, and Characterization, *Chem. Rev.*, 2020, **120**(5), 2693–2758.

3 J. Zaumseil, Luminescent Defects in Single-Walled Carbon Nanotubes for Applications. Adv, *Opt. Mater.*, 2022, **10**, 2101576.

4 G. Hong, S. Diao, A. L. Antaris and H. Dai, Carbon Nanomaterials for Biological Imaging and Nanomedicinal Therapy, *Chem. Rev.*, 2015, **115**(19), 10816–10906.

5 A. V. Naumov, D. A. Tsyboulski, S. M. Bachilo and R. B. Weisman, Length-dependent optical properties of single-walled carbon nanotube samples, *Chem. Phys.*, 2013, **422**, 255–263.

6 J. A. Fagan, J. R. Simpson, B. J. Bauer, S. H. De Paoli Lacerda, M. L. Becker, J. Chun, K. B. Migler, A. R. Hight Walker and E. K. Hobbie, Length-Dependent Optical Effects in Single-Wall Carbon Nanotubes, *J. Am. Chem. Soc.*, 2007, **129**(34), 10607–10612.

7 D. A. Heller, R. M. Mayrhofer, S. Baik, Y. V. Grinkova, M. L. Usrey and M. S. Strano, Concomitant Length and Diameter Separation of Single-Walled Carbon Nanotubes, *J. Am. Chem. Soc.*, 2004, **126**(44), 14567–14573.

8 A. Graf, Y. Zakharko, S. P. Schießl, C. Backes, M. Pfohl, B. S. Flavel and J. Zaumseil, Large scale, selective dispersion of long single-walled carbon nanotubes with high photoluminescence quantum yield by shear force mixing, *Carbon*, 2016, **105**, 593–599.

9 T. Hertel, S. Himmelein, T. Ackermann, D. Stich and J. Crochet, Diffusion Limited Photoluminescence Quantum Yields in 1-D Semiconductors: Single-Wall Carbon Nanotubes, *ACS Nano*, 2010, **4**(12), 7161–7168.

10 A. Krishnan, E. Dujardin, T. W. Ebbesen, P. N. Yianilos and M. M. J. Treacy, Young's modulus of single-walled nanotubes, *Phys. Rev. B: Condens. Matter Mater. Phys.*, 1998, **58**(20), 14013–14019.

11 D. Miyashiro, R. Hamano, H. Taira and K. Umemura, Analysis of vibration behavior in single strand DNA-wrapped single-walled carbon nanotubes adhered to lipid membranes, *Forces Mech.*, 2021, **2**, 100008.

12 D. Miyashiro, H. Taira, R. Hamano, R. L. Reserva and K. Umemura, Mechanical vibration of single-walled carbon nanotubes at different lengths and carbon nanobelts by modal analysis method, *Compos., Part C: Open Access*, 2020, **2**, 100028.

13 Y. Miyata, K. Shiozawa, Y. Asada, Y. Ohno, R. Kitaura, T. Mizutani and H. Shinohara, Length-sorted semiconducting carbon nanotubes for high-mobility thin film transistors, *Nano Res.*, 2011, **4**(10), 963–970.

14 F. Hennrich, W. Li, R. Fischer, S. Lebedkin, R. Krupke and M. M. Kappes, Length-Sorted, Large-Diameter, Polyfluorene-Wrapped Semiconducting Single-Walled Carbon Nanotubes for High-Density, Short-Channel Transistors, *ACS Nano*, 2016, **10**(2), 1888–1895.

15 Y. Asada, Y. Miyata, K. Shiozawa, Y. Ohno, R. Kitaura, T. Mizutani and H. Shinohara, Thin-Film Transistors with Length-Sorted DNA-Wrapped Single-Wall Carbon Nanotubes, *J. Phys. Chem. C*, 2011, **115**(1), 270–273.

16 M. Gaumet, A. Vargas, R. Gurny and F. Delie, Nanoparticles for drug delivery: the need for precision in reporting particle size parameters, *Eur. J. Pharm. Biopharm.*, 2008, **69**(1), 1–9.

17 H. Jin, D. A. Heller, R. Sharma and M. S. Strano, Size-Dependent Cellular Uptake and Expulsion of Single-Walled Carbon

Nanotubes: Single Particle Tracking and a Generic Uptake Model for Nanoparticles, *ACS Nano*, 2009, **3**(1), 149–158.

18 B. Kang, S. Chang, Y. Dai, D. Yu and D. Chen, Cell response to carbon nanotubes: Size-dependent intracellular uptake mechanism and subcellular fate, *Small*, 2010, **6**(21), 2362–2366.

19 Y. Iizumi, M. Yudasaka, J. Kim, H. Sakakita, T. Takeuchi and T. Okazaki, Oxygen-doped carbon nanotubes for near-infrared fluorescent labels and imaging probes, *Sci. Rep.*, 2018, **8**(1), 6272.

20 Y. Yomogida, T. Tanaka, M. Zhang, M. Yudasaka, X. Wei and H. Kataura, Industrial-scale separation of high-purity single-chirality single-wall carbon nanotubes for biological imaging, *Nat. Commun.*, 2016, **7**, 12056.

21 J. T. Robinson, G. Hong, Y. Liang, B. Zhang, O. K. Yaghi and H. Dai, *In vivo* fluorescence imaging in the second near-infrared window with long circulating carbon nanotubes capable of ultrahigh tumor uptake, *J. Am. Chem. Soc.*, 2012, **134**(25), 10664–10669.

22 T. Takeuchi, Y. Iizumi, M. Yudasaka, S. Kizaka-Kondoh and T. Okazaki, Characterization and Biodistribution Analysis of Oxygen-Doped Single-Walled Carbon Nanotubes Used as *in Vivo* Fluorescence Imaging Probes, *Bioconjugate Chem.*, 2019, **30**(5), 1323–1330.

23 T. T. S. Lew, V. B. Koman, K. S. Silmore, J. S. Seo, P. Gordiichuk, S. Y. Kwak, M. Park, M. C. Ang, D. T. Khong, M. A. Lee, M. B. Chan-Park, N. H. Chua and M. S. Strano, Real-time detection of wound-induced H(2)O(2) signalling waves in plants with optical nanosensors, *Nat. Plants*, 2020, **6**(4), 404–415.

24 M. H. Wong, J. P. Giraldo, S. Y. Kwak, V. B. Koman, R. Sinclair, T. T. Lew, G. Bisker, P. Liu and M. S. Strano, Nitroaromatic detection and infrared communication from wild-type plants using plant nanobionics, *Nat. Mater.*, 2017, **16**(2), 264–272.

25 N. M. Iverson, P. W. Barone, M. Shandell, L. J. Trudel, S. Sen, F. Sen, V. Ivanov, E. Atolia, E. Farias, T. P. McNicholas, N. Reuel, N. M. Parry, G. N. Wogan and M. S. Strano, *In vivo* biosensing *via* tissue-localizable near-infrared-fluorescent single-walled carbon nanotubes, *Nat. Nanotechnol.*, 2013, **8**(11), 873–880.

26 E. Gonzalez-Grandio, G. S. Demirer, C. T. Jackson, D. Yang, S. Ebert, K. Molawi, H. Keller and M. P. Landry, Carbon nanotube biocompatibility in plants is determined by their surface chemistry, *J. Nanobiotechnol.*, 2021, **19**(1), 431.

27 A. Spreinat, M. M. Dohmen, J. Lüttgens, N. Herrmann, L. F. Klepzig, R. Nißler, S. Weber, F. A. Mann, J. Lauth and S. Kruss, Quantum Defects in Fluorescent Carbon Nanotubes for Sensing and Mechanistic Studies, *J. Phys. Chem. C*, 2021, **125**(33), 18341–18351.

28 M. Kim, C. Chen, P. Wang, J. J. Mulvey, Y. Yang, C. Wun, M. Antman-Passig, H.-B. Luo, S. Cho, K. Long-Roche, L. V. Ramanathan, A. Jagota, M. Zheng, Y. Wang and D. A. Heller, Detection of ovarian cancer *via* the spectral fingerprinting of quantum-defect-modified carbon nanotubes in serum by machine learning, *Nat. Biomed. Eng.*, 2022, **6**(3), 267–275.

29 M. Kim, C. Chen, Z. Yaari, R. Frederiksen, E. Randall, J. Wollowitz, C. Cupo, X. Wu, J. Shah, D. Worroll, R. E. Lagenbacher, D. Goerzen, Y.-M. Li, H. An, Y. Wang and D. A. Heller, Nanosensor-based monitoring of autophagy-associated lysosomal acidification *in vivo*, *Nat. Chem. Biol.*, 2023, **19**, 1448–1457.

30 J. T. Metternich, J. A. C. Wartmann, L. Sistemich, R. Nißler, S. Herbertz and S. Kruss, Near-Infrared Fluorescent Biosensors Based on Covalent DNA Anchors, *J. Am. Chem. Soc.*, 2023, **145**(27), 14776–14783.

31 H. Kwon, M. Kim, B. Meany, Y. Piao, L. R. Powell and Y. Wang, Optical Probing of Local pH and Temperature in Complex Fluids with Covalently Functionalized, Semiconducting Carbon Nanotubes, *J. Phys. Chem. C*, 2015, **119**(7), 3733–3739.

32 J. A. Fagan, M. L. Becker, J. Chun and E. K. Hobbie, Length Fractionation of Carbon Nanotubes Using Centrifugation, *Adv. Mater.*, 2008, **20**(9), 1609–1613.

33 J. A. Fagan, M. L. Becker, J. Chun, P. Nie, B. J. Bauer, J. R. Simpson, A. Hight-Walker and E. K. Hobbie, Centrifugal Length Separation of Carbon Nanotubes, *Langmuir*, 2008, **24**(24), 13880–13889.

34 C. Y. Khripin, N. Arnold-Medabalimi and M. Zheng, Molecular-Crowding-Induced Clustering of DNA-Wrapped Carbon Nanotubes for Facile Length Fractionation, *ACS Nano*, 2011, **5**(10), 8258–8266.

35 H. Gui, H. Chen, C. Y. Khripin, B. Liu, J. A. Fagan, C. Zhou and M. Zheng, A facile and low-cost length sorting of single-wall carbon nanotubes by precipitation and applications for thin-film transistors, *Nanoscale*, 2016, **8**(6), 3467–3473.

36 X. Huang, R. S. McLean and M. Zheng, High-Resolution Length Sorting and Purification of DNA-Wrapped Carbon Nanotubes by Size-Exclusion Chromatography, *Anal. Chem.*, 2005, **77**(19), 6225–6228.

37 C. Y. Khripin, X. Tu, J. M. Heddleston, C. Silvera-Batista, A. R. Hight Walker, J. Fagan and M. Zheng, High-Resolution Length Fractionation of Surfactant-Dispersed Carbon Nanotubes, *Anal. Chem.*, 2013, **85**(3), 1382–1388.

38 C. Y. Khripin, X. Tu, J. Howarter, J. Fagan and M. Zheng, Concentration Measurement of Length-Fractionated Colloidal Single-Wall Carbon Nanotubes, *Anal. Chem.*, 2012, **84**(20), 8733–8739.

39 N. Komatsu and F. Wang, A Comprehensive Review on Separation Methods and Techniques for Single-Walled Carbon Nanotubes, *Materials*, 2010, 3818–3844.

40 J. A. Fagan, B. J. Bauer, E. K. Hobbie, M. L. Becker, A. R. Hight Walker, J. R. Simpson, J. Chun, J. Obrzut, V. Bajpai, F. R. Phelan, D. Simien, J. Y. Huh and K. B. Migler, Carbon Nanotubes: Measuring Dispersion and Length, *Adv. Mater.*, 2011, **23**(3), 338–348.

41 S. Duesberg, G. Burghard, M. Muster and J. Philipp, Separation of carbon nanotubes by size exclusion chromatography, *Chem. Commun.*, 1998, (3), 435–436.

42 G. S. Duesberg, J. Muster, V. Krstic, M. Burghard and S. Roth, Chromatographic size separation of single-wall carbon nanotubes, *Appl. Phys. A: Mater. Sci. Process.*, 1998, **67**(1), 117–119.

43 Y. Miyauchi, K. Matsuda, Y. Yamamoto, N. Nakashima and Y. Kanemitsu, Length-Dependent Photoluminescence Lifetimes in Single-Walled Carbon Nanotubes, *J. Phys. Chem. C*, 2010, **114**(30), 12905–12908.

44 Y. Yamamoto, T. Fujigaya, Y. Niidome and N. Nakashima, Fundamental properties of oligo double-stranded DNA/single-walled carbon nanotube nanobiohybrids, *Nanoscale*, 2010, **2**(9), 1767–1772.

45 Y. Asada, T. Sugai, R. Kitaura and H. Shinohara, Chromatographic Length Separation and Photoluminescence Study on DNA-Wrapped Single-Wall and Double-Wall Carbon Nanotubes, *J. Nanomater.*, 2009, **2009**, 1–8.

46 M. L. Becker, J. A. Fagan, N. D. Gallant, B. J. Bauer, V. Bajpai, E. K. Hobbie, S. H. Lacerda, K. B. Migler and J. P. Jakupciak, Length-Dependent Uptake of DNA-Wrapped Single-Walled Carbon Nanotubes, *Adv. Mater.*, 2007, **19**(7), 939–945.

47 X. Gong, A. K. Sharma, M. S. Strano and D. Mukhopadhyay, Selective Assembly of DNA-Conjugated Single-Walled Carbon Nanotubes from the Vascular Secretome, *ACS Nano*, 2014, **8**(9), 9126–9136.

48 M. Gravely, M. M. Safaee and D. Roxbury, Biomolecular Functionalization of a Nanomaterial To Control Stability and Retention within Live Cells, *Nano Lett.*, 2019, **19**(9), 6203–6212.

49 Y. Tsutsumi, T. Fujigaya and N. Nakashima, Size reduction of 3D-polymer-coated single-walled carbon nanotubes by ultracentrifugation, *Nanoscale*, 2015, **7**(46), 19534–19539.

50 Y. Tsutsumi, T. Fujigaya and N. Nakashima, Requirement for the Formation of Crosslinked Polymers on Single-walled Carbon Nanotubes Using Vinyl Monomers, *Chem. Lett.*, 2016, **45**(3), 274–276.

51 Y. Tsutsumi, T. Fujigaya and N. Nakashima, Polymer synthesis inside a nanospace of a surfactant–micelle on carbon nanotubes: creation of highly-stable individual nanotubes/ultrathin cross-linked polymer hybrids, *RSC Adv.*, 2014, **4**, 6318–6323.

52 Y. Nagai, Y. Tsutsumi, N. Nakashima and T. Fujigaya, Synthesis of Single-Walled Carbon Nanotubes Coated with Thiol-Reactive Gel *via* Emulsion Polymerization, *J. Am. Chem. Soc.*, 2018, **140**(27), 8544–8550.

53 Y. Nagai, K. Nakamura, M. Yudasaka, T. Shiraki and T. Fujigaya, Radical Polymer Grafting on the Surface of Single-Walled Carbon Nanotubes Enhances Photoluminescence in the Near-Infrared Region: Implications for Bioimaging and Biosensing, *ACS Appl. Nano Mater.*, 2020, **3**(9), 8840–8847.

54 S. S. Y. Law, G. Liou, Y. Nagai, J. Gimenez-Dejoz, A. Tateishi, K. Tsuchiya, Y. Kodama, T. Fujigaya and K. Numata, Polymer-coated carbon nanotube hybrids with functional peptides for gene delivery into plant mitochondria, *Nat. Commun.*, 2022, **13**(1), 2417.

55 Y. Nagai, M. Yudasaka, H. Kataura and T. Fujigaya, Brighter near-IR emission of single-walled carbon nanotubes modified with a cross-linked polymer coating, *Chem. Commun.*, 2019, **55**(48), 6854–6857.

56 Y. Nagai, K. Nakamura, J. Ohno, M. Kawaguchi and T. Fujigaya, Antibody-Conjugated Gel-Coated Single-Walled Carbon Nanotubes as Photothermal Agents, *ACS Appl. Bio. Mater.*, 2021, **4**(6), 5049–5056.

57 Y. Nagai, R. Hamano, K. Nakamura, I. A. Widjaja, N. Tanaka, M. Zhang, T. Tanaka, H. Kataura, M. Yudasaka and T. Fujigaya, Bright NIR-II fluorescence from biocompatible gel-coated carbon nanotubes for *in vivo* imaging, *Carbon*, 2024, **218**, 118728.

58 Y. Niidome, R. Hamano, K. Nakamura, S. Qi, S. Ito, B. Yu, Y. Nagai, N. Tanaka, T. Mori, Y. Katayama, T. Fujigaya and T. Shiraki, Near-infrared photoluminescent detection of serum albumin using single-walled carbon nanotubes locally functionalized with a long-chain fatty acid, *Carbon*, 2024, **216**, 118533.

59 F. Schöppler, C. Mann, T. C. Hain, F. M. Neubauer, G. Privitera, F. Bonaccorso, D. Chu, A. C. Ferrari and T. Hertel, Molar Extinction Coefficient of Single-Wall Carbon Nanotubes, *J. Phys. Chem. C*, 2011, **115**(30), 14682–14686.

60 F. A. Mann, P. Galonska, N. Herrmann and S. Kruss, Quantum defects as versatile anchors for carbon nanotube functionalization, *Nat. Protoc.*, 2022, **17**(3), 727–747.

61 M. Zheng, A. Jagota, E. D. Semke, B. A. Diner, R. S. McLean, S. R. Lustig, R. E. Richardson and N. G. Tassi, DNA-assisted dispersion and separation of carbon nanotubes, *Nat. Mater.*, 2003, **2**(5), 338–342.

62 Y. Noguchi, T. Fujigaya, Y. Niidome and N. Nakashima, Single-walled carbon nanotubes/DNA hybrids in water are highly stable, *Chem. Phys. Lett.*, 2008, **455**(4–6), 249–251.

63 A. Gandini, D. Coelho, M. Gomes, B. Reis and A. Silvestre, Materials from renewable resources based on furan monomers and furan chemistry: work in progress, *J. Mater. Chem.*, 2009, **19**, 8656–8664.

64 S. G. Chou, H. Son, J. Kong, A. Jorio, R. Saito, M. Zheng, G. Dresselhaus and M. S. Dresselhaus, Length characterization of DNA-wrapped carbon nanotubes using Raman spectroscopy, *Appl. Phys. Lett.*, 2007, **90**(13), 131109.

65 Y. Piao, B. Meany, L. R. Powell, N. Valley, H. Kwon, G. C. Schatz and Y. Wang, Brightening of carbon nanotube photoluminescence through the incorporation of sp^3 defects, *Nat. Chem.*, 2013, **5**(10), 840–845.

66 A. K. Wright and M. R. Thompson, Hydrodynamic structure of bovine serum albumin determined by transient electric birefringence, *Biophys. J.*, 1975, **15**(2, Part 1), 137–141.